JOURNAL OF GUIDANCE, CONTROL, AND DYNAMICS
Vol. 18, No. 6, November–December 1995

Aerocapture with a Flexible Tether

Jordi Puig-Suari, James M. Longuski, and Steven G. Tragesser
Purdue University, West Lafayette, Indiana 47907-1282

In previous work, the authors have demonstrated that the aerobraking tether, modeled as a rigid rod, could achieve aerocapture at any atmosphere-bearing planet in the solar system for less mass than the corresponding propellant of a typical retro-rocket system. In this paper, the great promise of the aerobraking tether is further explored by developing the equations of motion for the analysis of flexible tether behavior during the maneuver. A standard Lagrangian approach is taken with the tether modeled as a chain of linked rigid rods. Since an arbitrary number of rods can be used, the flexible behavior can be approximated to an arbitrary degree of accuracy. The results indicate that the aerobraking tether concept remains feasible when flexibility effects are included in the model.

Introduction

IN recent years, with new developments in tether technology, the use of tethered spacecraft in an atmosphere has received much attention from the scientific community.[1–6] The research areas have addressed a wide range of interesting topics such as upper atmosphere research,[2,3,5] equilibrium configurations,[3] and orbit decay.[4] With the exception of a paper describing the hypersonic parachute,[6] most of the literature on tethers in an atmosphere has been devoted to applications in which the aerodynamic forces are usually less significant than the gravitational forces. In this paper we analyze an application closely related to the hypersonic parachute, namely that of the aerobraking tether.

In the aerobraking maneuver, very large aerodynamic forces (significantly greater than the force of gravity) are required to decelerate the vehicle into a capture orbit about the target planet (Fig. 1). The model used in the earlier analyses[7–12] assumed a rigid tether, planar motion, and an exponential atmosphere. The results obtained with this simplified model were very encouraging and indicated that performing aerobraking maneuvers with tethered spacecraft is feasible. In the next step we extend the analysis to include the effect of a flexible tether. Before doing so, we briefly review the basic assumptions and results of the previous work.

Design Considerations and Rigid-Body Results

In Ref. 10 the possibility of using aerobraking tethers in the exploration of the atmosphere-bearing planets and satellites in the solar system is studied. The analysis includes missions to Venus, Mars, Jupiter, Saturn, Uranus, Neptune, and Titan and a Mars–Earth return

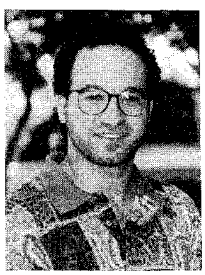

Jordi Puig-Suari received his B.S., M.S., and Ph.D. degrees in Aeronautical and Astronautical Engineering from Purdue University. In 1993–1994 he worked at Purdue as a Visiting Assistant Professor. In 1994 he joined the Department of Mechanical and Aerospace Engineering at Arizona State University as an Assistant Professor. His research interests include vehicle dynamics and control, aerospace systems design, and analysis of tethered satellites.

James M. Longuski received his B.S.E., M.S.E., and Ph.D. degrees in Aerospace Engineering at the University of Michigan. From 1979 to 1988 he worked at the Jet Propulsion Laboratory, spending three years in the Guidance and Control Section and six years in the Mission Design Section. In 1988 he accepted the position of Assistant Professor at Purdue University in the School of Aeronautics and Astronautics. He was promoted to Associate Professor in 1992. His research interests include analytic theory and control of rigid-body motion, analysis of tethers in space, and mission design. He is an Associate Fellow of the AIAA.

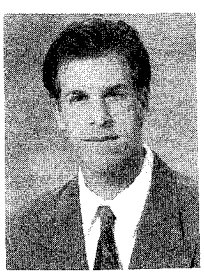

Steven G. Tragesser attended the U.S. Air Force Academy from 1988 through 1990 and obtained his Bachelor's degree in Aeronautical and Astronautical Engineering from the University of Illinois in 1992. He received his Master's degree in Aeronautical and Astronautical Engineering from Purdue University in 1994, where he is currently pursuing his doctorate on the use of tethers in aerobraking maneuvers.

Received Feb. 4, 1994; revision received April 10, 1995; accepted for publication June 2, 1995.

Table 1 Aerocapture results for solar system exploration

Parameter	Venus	Earth	Mars	Jupiter	Saturn	Uranus	Neptune	Titan
ΔV, km/s	0.35	0.39	0.67	0.27	0.41	0.50	0.34	1.31
Propellant mass, kg	126	142	256	96	149	185	122	559
Tether mass, kg	31	38	112	18	42	63	29	426
Savings, %	75	73	56	81	72	66	76	24
Savings, kg	95	104	144	78	107	122	93	133
Length, km	10.8	9.0	14.5	36.1	54.4	72.7	72.7	84.2
Diameter, mm	1.42	1.73	2.34	0.60	0.74	0.78	0.53	1.89
Probe area, m^2	999	818	605	2,370	1,910	1,810	2,670	747
Design tension, N	5,670	8,450	15,500	1,010	1,550	1,720	795	10,100
Actual tension, N	5,500	7,860	12,700	1,050	1,630	1,860	899	9,700
Percentage of design	97	93	82	104	105	108	113	96

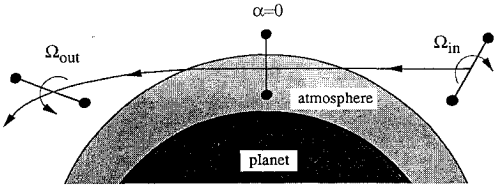

Fig. 1 Aerobraking maneuver.

mission. In this preliminary study, certain specifications were made that ultimately led to unique designs for each tether mission. These specifications include the following:

1) The fly-through maneuver (Fig. 1) is designed so that the tether achieves a vertical orientation at closest approach. In addition, the inertial spin rate before atmospheric entry, Ω_{in}, is equal and opposite to the spin rate after exit, Ω_{out}:

$$\Omega_{out} = -\Omega_{in} \tag{1}$$

This requirement is called spin matching.

2) The tether length is specified so that the location of the center of pressure, l_{ps}, is equal to that of the center of percussion, l_{pc}. This requirement is called center matching:

$$l_{ps} = l_{pc} \tag{2}$$

Note that the location of the center of percussion is only a function of the length of the tether and the mass ratio of the orbiter and the probe. On the other hand, the position of the center of pressure is primarily a function of the scale height of the atmosphere. This makes the center matching condition relatively insensitive to variations in atmospheric density or small changes in scale height.

3) The ballistic coefficient of the probe is equal to the ballistic coefficient of the tether:

$$\eta/(C_{D_t}d) = m_p/(C_{D_p}S_p) \tag{3}$$

where η is the tether linear density, which depends on the tether mass and length; C_{D_t} and C_{D_p} are the drag coefficients of the tether and the probe, respectively; d is the diameter of the tether; and S_p is the frontal area of the probe. The values assumed for C_{D_t} and C_{D_p} are 2 and 1, respectively.[10] This requirement is called aeromatching.

4) The mass of the orbiter, m_o, and the mass of the probe, m_p, are both assumed to be equal to 1000 kg.

5) The tether is assumed to be made of Hercules AS4 graphite with a tensile strength σ_u of 3.6 GN/m^2 and a density ρ_t of 1800 kg/m^3.

6) The planets are assumed to be in circular, coplanar orbits. Arrival conditions are calculated by assuming an interplanetary Hohmann transfer into a near-parabolic capture orbit about the target planet ($e < 1$).

From condition (1), it can be shown[10] that the mass of the tether is given by

$$M = \frac{\rho_t m_o(m_o + m_p)}{4\sigma_u m_p}\Delta V^2 \tag{4}$$

where ΔV is the change in velocity required at closest approach of the target planet in order to achieve capture.

In Ref. 10 a comparison is made between the mass of the tether (4) and the propellant mass required (to slow down the orbiter) with a chemical rocket system, Δm:

$$\Delta m = m_f(e^{\Delta V/I_{sp}g} - 1) \tag{5}$$

where g is the acceleration due to gravity at the Earth's surface, m_f is the final mass of the orbiter, and Δm is the propellant mass. The value for I_{sp} is assumed to be 300 s. The results of this comparison, presented in Table 1, are quite exciting because in every case the tether mass is smaller than the required propellant mass. The greatest absolute savings are at Mars (144 kg) and the greatest percentage savings are at Jupiter (81%). The design tension, computed by the simple formula[10]

$$T = \frac{m_o(m_o + m_p)}{4m_p l}\Delta V^2 \tag{6}$$

is a very good approximation to the actual tension observed in the simulation of the fly-through maneuver.

The promising results obtained for the rigid-rod model and summarized in Table 1 demand that a deeper examination of the potential of aerobraking tethers be made. In the above analysis, the tether is modeled as a rigid rod but is designed [by conditions (2) and (3)] to minimize normal forces. The next logical step is to introduce a flexible tether model to test the virtue of the aforementioned designs. In addition, a flexible model will allow a study of how variations in the design will affect normal forces, bending, and aerodynamic forces.

Of primary concern are the following questions. Will the bending behavior of the tether invalidate the assumptions and conclusions made with the rigid-rod model? For example, if the tether bends significantly, the drag forces may be dramatically altered. Bending can also raise the periapsis of the probe, causing it to miss the target altitude and, hence, not achieve aerocapture. Can elastic stretching cause the reverse effect? If the tether stretches significantly, it may drop the probe too deeply into the atmosphere, perhaps resulting in a crash instead of the intended capture orbit. Finally, what happens if the matching conditions (2) and (3) are not adhered to? Are they required for a well-behaved aerocapture maneuver?

Planar Flexible Model

The flexible model developed in this paper approximates the flexible tether as a chain of linked rigid rods with the end masses modeled as particles (see Fig. 2). This makes full use of the rigid-rod model previously developed,[7] which includes an aerodynamic model for the distributed forces along the tether. This integrated modeling of the aerodynamic forces is fundamental in the analysis of the aerobraking problem where large changes in velocity and atmospheric density occur along the tether. The linked rigid-rod model also provides an accurate description of the inertial and gravitational forces on the tether. In addition, the model includes a spring damper at the orbiter end of the tether that can be used to approximately model the elastic behavior (stretching) of either the tether or a shock absorber at the orbiter attachment point. The number of rods and the length of each rod are arbitrary, so that flexible effects can be modeled to any

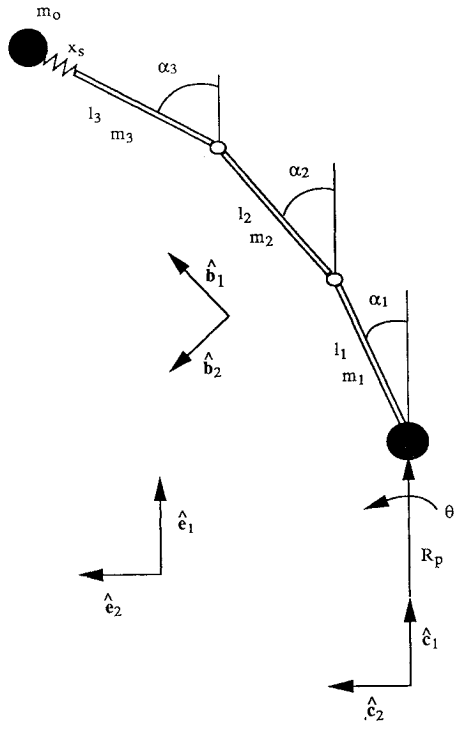

Fig. 2 Generalized coordinates for flexible tether system.

desired degree of accuracy. Changing the length of the rods along the tether allows an increase in accuracy in the portion of the tether where the flexible effects are most significant. The motion of the system is constrained to the plane of the orbit, as in the rigid-rod model. Finally, the orbit is assumed to be equatorial. This model should permit adequate analysis of the bending and stretching behavior of the tether and thus allow us to address questions raised about the rigid-rod analysis.

Lagrange's Equations of Motion

The equations of motion will be found by Lagrange's equations, written in the form[13]

$$\frac{\mathrm{d}}{\mathrm{d}t}\left(\frac{\partial T}{\partial \dot{q}_i}\right) - \frac{\partial T}{\partial q_i} + \frac{\partial V}{\partial q_i} = Q_i \tag{7}$$

where the Q_i are generalized forces not derivable from a potential function (i.e., the aerodynamic and damping forces). This form of Lagrange's equations is used because the potential energy of the system, V, is not a function of $\dot{q}$. The use of Lagrange's equations facilitates the derivation of equations for an arbitrary number of tether elements by eliminating the internal forces between the rods from the analysis. The generalized coordinates in the system are the orientation α_i of each rod, the position coordinates of the probe, R_p and θ, and the elongation of the spring, x_s (see Fig. 2).

Kinetic Energy

From Fig. 2 we see that the radial position vector $\boldsymbol{R}_{cmi}$ from the center of the planet to the center of mass of the ith rod (assuming each rod is uniform) is given as

$$\boldsymbol{R}_{cmi} = \left(R_p + \sum_{n=1}^{i-1} l_n C\alpha_n + \frac{l_i}{2} C\alpha_i\right)\hat{\boldsymbol{c}}_1 + \left(\sum_{n=1}^{i-1} l_n S\alpha_n + \frac{l_i}{2} S\alpha_i\right)\hat{\boldsymbol{c}}_2 \tag{8}$$

where $C\alpha \equiv \cos\alpha$ and $S\alpha \equiv \sin\alpha$. Noting that the angular velocity of reference frame $\hat{\boldsymbol{c}}$ with respect to inertial frame $\hat{\boldsymbol{e}}$ is

$${}^{e}\boldsymbol{\omega}^{c} = \dot{\theta}\hat{\boldsymbol{c}}_3 \tag{9}$$

the inertial velocity of the center of mass of each rod, $\boldsymbol{v}_{cmi}$, is given by

$$\boldsymbol{v}_{cmi} = \left[\dot{R}_p - \sum_{n=1}^{i-1} l_n(\dot{\alpha}_n + \dot{\theta})S\alpha_n - \frac{l_i}{2}(\dot{\alpha}_i + \dot{\theta})S\alpha_i\right]\hat{\boldsymbol{c}}_1 + \left[R_p\dot{\theta} + \sum_{n=1}^{i-1} l_n(\dot{\alpha}_n + \dot{\theta})C\alpha_n + \frac{l_i}{2}(\dot{\alpha}_i + \dot{\theta})C\alpha_i\right]\hat{\boldsymbol{c}}_2 \tag{10}$$

Thus the total kinetic energy of the tether, T_t, for N rods is given by

$$T_t = \sum_{i=1}^{N} \frac{1}{2} m_i \boldsymbol{v}_{cmi} \cdot \boldsymbol{v}_{cmi} + \frac{m_i l_i^2}{24}(\dot{\alpha}_i + \dot{\theta})^2 \tag{11}$$

where the last term on the right-hand side is the rotational kinetic energy. Similarly, the radial position vectors to the probe, $\boldsymbol{R}_p$, and to the orbiter, $\boldsymbol{R}_o$, are given by

$$\boldsymbol{R}_p = R_p\hat{\boldsymbol{c}}_1 \tag{12}$$

$$\boldsymbol{R}_o = \left(R_p + \sum_{n=1}^{N} l_n C\alpha_n + x_s C\alpha_N\right)\hat{\boldsymbol{c}}_1 + \left(\sum_{n=1}^{N} l_n S\alpha_n + x_s S\alpha_N\right)\hat{\boldsymbol{c}}_2 \tag{13}$$

Thus, the inertial velocities of the probe, $\boldsymbol{v}_p$, and the orbiter, $\boldsymbol{v}_o$, are

$$\boldsymbol{v}_p = \dot{R}_p\hat{\boldsymbol{c}}_1 + R_p\dot{\theta}\hat{\boldsymbol{c}}_2 \tag{14}$$

$$\boldsymbol{v}_o = \left[\dot{R}_p - \sum_{n=1}^{N}(l_n + x_s\delta_{nN})(\dot{\alpha}_n + \dot{\theta})S\alpha_n + \dot{x}_s C\alpha_N\right]\hat{\boldsymbol{c}}_1 + \left[R_p\dot{\theta} + \sum_{n=1}^{N}(l_n + x_s\delta_{nN})(\dot{\alpha}_n + \dot{\theta})C\alpha_n + \dot{x}_s S\alpha_N\right]\hat{\boldsymbol{c}}_2 \tag{15}$$

where δ_{nN} is the Kronecker delta. The kinetic energies of the probe, T_p, and the orbiter, T_o, are given as

$$T_p = \tfrac{1}{2} m_p \boldsymbol{v}_p \cdot \boldsymbol{v}_p, \qquad T_o = \tfrac{1}{2} m_o \boldsymbol{v}_o \cdot \boldsymbol{v}_o \tag{16}$$

Finally, we have the total kinetic energy of the tethered system:

$$T = T_t + T_p + T_o \tag{17}$$

Potential Energy

The potential energy V of a Newtonian gravity field is given by

$$V = -\mu(m/R) \tag{18}$$

where μ is the gravitational constant of the planet, m is the mass of a particle, and R is the radial distance from the center of the planet to the particle. The potential energy of the ith rod is given by

$$V_i = -\mu\eta_i \int_0^{l_i} \frac{\mathrm{d}\xi}{R_{\xi i}} \tag{19}$$

where η is the linear density of the rod, assumed constant, and $R_{\xi i}$ is the radial distance from the center of the planet to a differential element located at a distance ξ along the ith rod. Thus, we have

$$\boldsymbol{R}_{\xi i} = \left(R_p + \sum_{n=1}^{i-1} l_n C\alpha_n + \xi C\alpha_i\right)\hat{\boldsymbol{c}}_1 + \left(\sum_{n=1}^{i-1} l_n S\alpha_n + \xi S\alpha_i\right)\hat{\boldsymbol{c}}_2 \tag{20}$$

$$R_{\xi i}^2 = R_p^2 + \sum_{n=1}^{i-1}\left[2R_p l_n C\alpha_n + \sum_{k=1}^{i-1} l_n l_k (C\alpha_n C\alpha_k + S\alpha_n S\alpha_k)\right]$$

$$+2\left[R_p C\alpha_i + \sum_{n=1}^{i-1} l_n (C\alpha_n C\alpha_i + S\alpha_n S\alpha_i)\right]\xi + \xi^2$$

$$= a_i + b_i\xi + \xi^2 \tag{21}$$

and the potential energy of the ith rod, V_i, is given by the integral

$$V_i = -\mu\eta_i \int_0^{l_i} \frac{\mathrm{d}\xi}{\sqrt{a_i + b_i\xi + \xi^2}} \tag{22}$$

Solving (22) and summing over all N rods, we find that the total potential energy of the tether, V_t (not including the orbiter and probe), is

$$V_t = -\mu \sum_{i=1}^{N} \eta_i \ell n\left(\frac{2\sqrt{a_i + b_i l_i + l_i^2} + 2l_i + b_i}{2\sqrt{a_i} + b_i}\right) \tag{23}$$

Since the probe and the orbiter are modeled as particles, their potential energies V_p and V_o, respectively, are given by

$$V_p = -\mu(m_p/R_p), \qquad V_o = -\mu(m_o/R_o) \tag{24}$$

The potential energy stored in the spring is

$$V_s = \tfrac{1}{2}kx_s^2 \tag{25}$$

where k is the spring constant. Finally, the total potential energy of the system is

$$V = V_t + V_p + V_o + V_s \tag{26}$$

Generalized Forces

We model the aerodynamic drag as

$$\boldsymbol{F} = -\tfrac{1}{2}\rho C_D S v \boldsymbol{v} \tag{27}$$

where C_D is the drag coefficient, S is the frontal area of the body, $\boldsymbol{v}$ is the velocity with respect to the atmosphere (the wind), and ρ is the atmospheric density given as

$$\rho = \rho_r e^{(h_r + R_{\mathrm{pl}} - R)/H} \tag{28}$$

where ρ_r is the reference density at the reference altitude h_r, R_{pl} is the radius of the planet, and H is the scale height corresponding to ρ_r.

Assuming that the atmosphere rotates with the planet at a rate Ω, we find that the velocity of the atmosphere (wind) with respect to the probe, $\boldsymbol{v}_{wp}$, is given by

$$\boldsymbol{v}_{wp} = \dot{R}_p\hat{\boldsymbol{c}}_1 + R_p(\dot{\theta} - \Omega)\hat{\boldsymbol{c}}_2 \tag{29}$$

Thus, the aerodynamic force on the probe, from Eqs. (27–29), is

$$\boldsymbol{F}_p = -\tfrac{1}{2}\rho_p C_{D_p} S_p \sqrt{\boldsymbol{v}_{wp}\cdot\boldsymbol{v}_{wp}}[\dot{R}_p\hat{\boldsymbol{c}}_1 + R_p(\dot{\theta} - \Omega)\hat{\boldsymbol{c}}_2] \tag{30}$$

Similarly, the velocity of the atmosphere with respect to the orbiter, $\boldsymbol{v}_{wo}$, is given as

$$\boldsymbol{v}_{wo} = \left[\dot{R}_p - \sum_{n=1}^{N}(l_n + x_s\delta_{nN})(\dot{\alpha}_n + \dot{\theta} - \Omega)S\alpha_n + \dot{x}_s C\alpha_N\right]\hat{\boldsymbol{c}}_1$$

$$+\left[R_p(\dot{\theta} - \Omega) + \sum_{n=1}^{N}(l_n + x_s\delta_{nN})(\dot{\alpha}_n + \dot{\theta} - \Omega)C\alpha_n + \dot{x}_s S\alpha_N\right]\hat{\boldsymbol{c}}_2 \tag{31}$$

and the aerodynamic force on the orbiter, $\boldsymbol{F}_o$, is given by

$$\boldsymbol{F}_o = -\frac{1}{2}\rho_o C_{D_o} S_o \sqrt{\boldsymbol{v}_{wo}\cdot\boldsymbol{v}_{wo}}$$

$$\times\left\{\left[\dot{R}_p - \sum_{n=1}^{N}(l_n + x_s\delta_{nN})(\dot{\alpha}_n + \dot{\theta} - \Omega)S\alpha_n + \dot{x}_s C\alpha_N\right]\hat{\boldsymbol{c}}_1\right.$$

$$\left.+\left[R_p(\dot{\theta} - \Omega) + \sum_{n=1}^{N}(l_n + x_s\delta_{nN})(\dot{\alpha}_n + \dot{\theta} - \Omega)C\alpha_n + \dot{x}_s S\alpha_N\right]\hat{\boldsymbol{c}}_2\right\} \tag{32}$$

To obtain the generalized forces on the probe and the orbiter, we use[13]

$$Q_i = \sum_{k=1}^{n} \boldsymbol{F}_k \cdot \frac{\partial \boldsymbol{R}_k}{\partial q_i} \tag{33}$$

where $\boldsymbol{R}_k$ must be written in inertial coordinates. Using the $\hat{\boldsymbol{e}}$ frame in Fig. 2 as the inertial reference, we have, for the probe,

$$\boldsymbol{R}_p = R_p\hat{\boldsymbol{c}}_1 = R_p(C\theta\hat{\boldsymbol{e}}_1 + S\theta\hat{\boldsymbol{e}}_2) \tag{34}$$

$$\boldsymbol{F}_p = F_{p1}\hat{\boldsymbol{c}}_1 + F_{p2}\hat{\boldsymbol{c}}_2 = (F_{p1}C\theta - F_{p2}S\theta)\hat{\boldsymbol{e}}_1$$

$$+(F_{p1}S\theta + F_{p2}C\theta)\hat{\boldsymbol{e}}_2 \tag{35}$$

and the generalized forces on the probe are

$$Q_{Rpp} = \boldsymbol{F}_p \cdot \frac{\partial \boldsymbol{R}_p}{\partial R_p} = F_{p1}, \qquad Q_{\theta p} = \boldsymbol{F}_p \cdot \frac{\partial \boldsymbol{R}_p}{\partial \theta} = F_{p2}R_p$$
$$Q_{\alpha jp} = Q_{xsp} = 0 \tag{36}$$

Similarly, for the orbiter we have

$$\boldsymbol{R}_o = \left(R_p + \sum_{n=1}^{N} l_n C\alpha_n + x_s C\alpha_N\right)\hat{\boldsymbol{c}}_1$$

$$+\left(\sum_{n=1}^{N} l_n S\alpha_n + x_s S\alpha_N\right)\hat{\boldsymbol{c}}_2$$

$$= \left[R_p C\theta + \sum_{n=1}^{N}(l_n + x_s\delta_{nN})(C\alpha_n C\theta - S\alpha_n S\theta)\right]\hat{\boldsymbol{e}}_1$$

$$+\left[R_p S\theta + \sum_{n=1}^{N}(l_n + x_s\delta_{nN})(C\alpha_n S\theta + S\alpha_n C\theta)\right]\hat{\boldsymbol{e}}_2 \tag{37}$$

$$\boldsymbol{F}_o = F_{o1}\hat{\boldsymbol{c}}_1 + F_{o2}\hat{\boldsymbol{c}}_2 = (F_{o1}C\theta - F_{o2}S\theta)\hat{\boldsymbol{e}}_1 + (F_{o1}S\theta + F_{o2}C\theta)\hat{\boldsymbol{e}}_2 \tag{38}$$

and so, the generalized forces on the orbiter are

$$Q_{Rpo} = \boldsymbol{F}_p \cdot \frac{\partial \boldsymbol{R}_o}{\partial R_p} = F_{o1} \tag{39}$$

$$Q_{\theta o} = \boldsymbol{F}_o \cdot \frac{\partial \boldsymbol{R}_o}{\partial \theta} = R_p F_{o2}$$

$$+\sum_{n=1}^{N}(l_n + x_s\delta_{nN})(-F_{o1}S\alpha_n + F_{o2}C\alpha_n) \tag{40}$$

$$Q_{\alpha jo} = \boldsymbol{F}_o \cdot \frac{\partial \boldsymbol{R}_o}{\partial \alpha_j} = (l_j + x_s\delta_{jN})(-F_{o1}S\alpha_j + F_{o2}C\alpha_j) \tag{41}$$

$$Q_{xso} = \boldsymbol{F}_o \cdot \frac{\partial \boldsymbol{R}_o}{\partial x_s} = F_{o1}C\alpha_N + F_{o2}S\alpha_N \tag{42}$$

The analysis of the aerodynamic force on the tether is more complicated because each point of the tether is located at a different altitude, so the density of the atmosphere varies along the tether length, and also because each point of the tether is moving at a different velocity with respect to the atmosphere. The differential force $\mathrm{d}\boldsymbol{F}_i$ on the ith rod can be written as

$$\mathrm{d}\boldsymbol{F}_i = -\tfrac{1}{2}\rho_{\xi i} C_D v_{w\xi i} \boldsymbol{v}_{w\xi i}\, \mathrm{d}S_\perp \tag{43}$$

where $\rho_{\xi i}$ is the atmospheric density at a distance ξ along the ith rod, $\boldsymbol{v}_{w\xi i}$ is the velocity of the point at ξ on the ith rod with respect to the atmosphere, and as in the rigid-rod model,[7] $\mathrm{d}S_\perp$ is the cross-sectional differential area projected perpendicular to the wind direction. The velocity $\boldsymbol{v}_{w\xi i}$ can be written as

$$\begin{aligned}\boldsymbol{v}_{w\xi i} &= \left[\dot{R}_p - \sum_{n=1}^{i-1} l_n(\dot{\alpha}_n + \dot{\theta} - \Omega) S\alpha_n \right.\\ &\quad \left. - \xi(\dot{\alpha}_i + \dot{\theta} - \Omega) S\alpha_i \right]\hat{\boldsymbol{c}}_1\\ &\quad + \left[R_p(\dot{\theta} - \Omega) + \sum_{n=1}^{i-1} l_n(\dot{\alpha}_n + \dot{\theta} - \Omega) C\alpha_n \right.\\ &\quad \left. + \xi(\dot{\alpha}_i + \dot{\theta} - \Omega) C\alpha_i \right]\hat{\boldsymbol{c}}_2\\ &= (B_1 - B_2\xi)\hat{\boldsymbol{c}}_1 + (B_3 + B_4\xi)\hat{\boldsymbol{c}}_2 \end{aligned} \tag{44}$$

where the B_j coefficients are introduced for convenience. The differential area $\mathrm{d}S_\perp$ is

$$\mathrm{d}S_\perp = \mathrm{sgn}(\boldsymbol{v}_{w\xi i} \cdot \hat{\boldsymbol{b}}_2) \frac{\boldsymbol{v}_{w\xi i} \cdot \hat{\boldsymbol{b}}_2}{v_{w\xi i}} d_i\, \mathrm{d}\xi \tag{45}$$

where d_i is the diameter of the ith rod and the body frame $\hat{\boldsymbol{b}}$ is defined in Fig. 2 ($\hat{\boldsymbol{b}}_1$ is along the tether and $\hat{\boldsymbol{b}}_2$ is normal to the tether). Substituting Eq. (45) into Eq. (43), we have

$$\mathrm{d}\boldsymbol{F}_i = -\tfrac{1}{2}\rho_{\xi i} C_D [\mathrm{sgn}(\boldsymbol{v}_{w\xi i} \cdot \hat{\boldsymbol{b}}_2) \boldsymbol{v}_{w\xi i} \cdot \hat{\boldsymbol{b}}_2 d_i] \boldsymbol{v}_{w\xi i}\, \mathrm{d}\xi \tag{46}$$

where

$$\begin{aligned}\boldsymbol{v}_{w\xi i} \cdot \hat{\boldsymbol{b}}_2 &= \boldsymbol{v}_{w\xi i} \cdot (C\alpha_i \hat{\boldsymbol{c}}_2 - S\alpha_i \hat{\boldsymbol{c}}_1) = R_p(\dot{\theta} - \Omega) C\alpha_i - \dot{R}_p S\alpha_i\\ &\quad + \sum_{n=1}^{i-1} l_n(\dot{\alpha}_n + \dot{\theta} - \Omega)(S\alpha_n S\alpha_i + C\alpha_n C\alpha_i) + \xi(\dot{\alpha}_i + \dot{\theta} - \Omega)\\ &= D_1 + D_2\xi \end{aligned} \tag{47}$$

and where the D_j coefficients are introduced for convenience. Evaluating the signum function in Eq. (46) and assuming that the function does not change sign along the ith rod, we have (by setting $\xi = 0$)

$$\mathrm{sgn}(\boldsymbol{v}_{w0i} \cdot \hat{\boldsymbol{b}}_2) = \mathrm{sgn}(D_1) = \sigma \tag{48}$$

which defines the symbol σ.

The assumption of an exponential atmosphere with constant scale height [Eq. (28)] results in the following expression for $\rho_{\xi i}$ in Eq. (46):

$$\rho_{\xi i} = \rho_r e^{(H_r + R_{\mathrm{pl}} - R_{\xi i})/H} = \rho_r e^{(H_r + R_{\mathrm{pl}})/H} e^{-R_{\xi i}/H} \tag{49}$$

where

$$e^{-R_{\xi i}/H} = \exp\left\{ \frac{\left[\left(R_p + \sum_{n=1}^{i-1} l_n C\alpha_n + \xi C\alpha_i\right)^2 + \left(\sum_{n=1}^{i-1} l_n S\alpha_n + \xi S\alpha_i\right)^2\right]^{\frac{1}{2}}}{H} \right\} \tag{50}$$

As discussed in Ref. 7, no closed-form expression in terms of elementary functions is possible for the integral $\int \mathrm{d}\boldsymbol{F}_i$ when Eq. (50) is substituted into Eq. (46). However, very accurate, approximate, closed-form expressions can be found by assuming that

$$\left(\frac{l_i S\alpha_i}{R_p}\right)^2 = 0 \tag{51}$$

so we have

$$e^{-R_{\xi i}/H} \approx \exp\left[\frac{-\left(R_p + \sum_{n=1}^{i-1} l_n C\alpha_n + \xi C\alpha_i\right)}{H} \right] \tag{52}$$

and Eq. (49) is approximated by

$$\begin{aligned}\rho_{\xi i} &\approx \rho_r \exp\left(\frac{H_r + R_{\mathrm{pl}} - R_p - \sum_{n=1}^{i-1} l_n C\alpha_n}{H} \right) e^{-\xi C\alpha_i/H}\\ &= K e^{-\xi C\alpha_i/H} \end{aligned} \tag{53}$$

where K is a convenient coefficient. Substituting Eqs. (44), (47), (48), and (53) into Eq. (46), we obtain the approximation

$$\begin{aligned}\mathrm{d}\boldsymbol{F}_i &= -\tfrac{1}{2} C_D d_i \sigma K (D_1 + D_2\xi)[(B_1 - B_2\xi)\hat{\boldsymbol{c}}_1\\ &\quad + (B_3 + B_4\xi)\hat{\boldsymbol{c}}_2] e^{-\xi C\alpha_i/H}\, \mathrm{d}\xi \end{aligned} \tag{54}$$

Integrating Eq. (54) and rearranging, we have

$$\begin{aligned}\boldsymbol{F}_i &= \int_0^{l_i} \mathrm{d}\boldsymbol{F}_i = -\frac{1}{2} C_D d_i \sigma K \{[D_1 B_1 I_0 + (D_2 B_1 - D_1 B_2) I_1\\ &\quad - B_2 D_2 I_2]\hat{\boldsymbol{c}}_1 + [D_1 B_3 I_0 + (D_2 B_3 + D_1 B_4) I_1 + B_4 D_2 I_2]\hat{\boldsymbol{c}}_2\} \end{aligned} \tag{55}$$

where

$$I_n \equiv \int_0^{l_i} \xi^n e^{-\xi C\alpha_i/H}\, \mathrm{d}\xi \tag{56}$$

which are known integrals.

Substituting Eqs. (54) and (20) into the generalized force expressions, we obtain the convenient forms

$$\begin{aligned}Q_{Rpi} &= \int_0^{l_i} \mathrm{d}\boldsymbol{F}_i \cdot \frac{\partial \boldsymbol{R}_{\xi i}}{\partial R_p}\\ &= -\frac{1}{2} C_D d_i \delta K [D_1 B_1 I_0 + (D_2 B_1 - D_1 B_2) I_1 - B_2 D_2 I_2] \end{aligned} \tag{57}$$

$$\begin{aligned}Q_{\theta i} &= \int_0^{l_i} \mathrm{d}\boldsymbol{F}_i \cdot \frac{\partial \boldsymbol{R}_{\xi i}}{\partial \theta}\\ &= -\frac{1}{2} C_D d_i \sigma K \left\{ -\sum_{n=1}^{i-1} l_n S\alpha_n [D_1 B_1 I_0 + (D_2 B_1 - D_1 B_2) I_1 \right.\\ &\quad - B_2 D_2 I_2] - S\alpha_i [D_1 B_1 I_1 + (D_2 B_1 - D_1 B_2) I_2 - B_2 D_2 I_3]\\ &\quad + \left(R_p + \sum_{n=1}^{i-1} l_n C\alpha_n\right)[D_1 B_3 I_0 + (D_2 B_3 + D_1 B_4) I_1\\ &\quad \left. + B_4 D_2 I_2] + C\alpha_i [D_1 B_3 I_1 + (D_2 B_3 + D_1 B_4) I_2 + B_4 D_2 I_3] \right\} \end{aligned} \tag{58}$$

$$\begin{aligned}Q_{\alpha j i} &= \int_0^{l_i} \mathrm{d}\boldsymbol{F}_i \cdot \frac{\partial \boldsymbol{R}_{\xi i}}{\partial \alpha_j} = -\frac{1}{2} C_D d_i \sigma K l_j\\ &\quad \times \{C\alpha_j [D_1 B_3 I_0 + (D_2 B_3 + D_1 B_4) I_1 + B_4 D_2 I_2] - S\alpha_j\\ &\quad \times [D_1 B_1 I_0 + (D_2 B_1 - D_1 B_2) I_1 - B_2 D_2 I_2]\} \qquad \text{for } j < i \end{aligned} \tag{59}$$

$$\begin{aligned}Q_{\alpha j i} &= \int_0^{l_i} \mathrm{d}\boldsymbol{F}_i \cdot \frac{\partial \boldsymbol{R}_{\xi i}}{\partial \alpha_i} = -\frac{1}{2} C_D d_i \sigma K\\ &\quad \times \{C\alpha_i [D_1 B_3 I_1 + (D_2 B_3 + D_1 B_4) I_2 + B_4 D_2 I_3] - S\alpha_i\\ &\quad \times [D_1 B_1 I_1 + (D_2 B_1 - D_1 B_2) I_2 - B_2 D_2 I_3]\} \qquad \text{for } j = 1 \end{aligned} \tag{60}$$

Finally, the generalized force for the damper, which appears only in the x_s equation, is

$$Q_c = -c\dot{x}_s \tag{61}$$

where c is the damping coefficient.

At this point, the equations of motion for the system are derived by using Lagrange's equations. The detailed derivation (which is too lengthy to be included here) is provided in Ref. 12.

Convenient Form for Equations of Motion

The form of the differential equations obtained by using Eqs. (7) is not convenient for numerical integration. This is because all the second-order terms $\ddot{R}_p$, $\ddot{\theta}$, and $\ddot{\alpha}_i$ appear in all the equations of motion.

In this section we discuss the derivation of the equations of motion for a system with an arbitrary number of rods N, keeping in mind that the desired form of the final differential equations should be

$$[A]\begin{Bmatrix} \ddot{q}_1 \\ \vdots \\ \ddot{q}_n \end{Bmatrix} = \{B\} \tag{62}$$

which can be rewritten as

$$\begin{Bmatrix} \ddot{q}_1 \\ \vdots \\ \ddot{q}_n \end{Bmatrix} = [A]^{-1}\{B\} \tag{63}$$

which is ideally suited for numerical integration.

Since all the terms containing second-order derivatives of the generalized coordinates $\ddot{q}$ can only arise from the $(\mathrm{d}/\mathrm{d}t)(\partial T/\partial \dot{q})$ terms of Eqs. (7), let us define

$$\frac{\mathrm{d}}{\mathrm{d}t}\left(\frac{\partial T}{\partial \dot{q}_j}\right) \equiv \bar{T}_{2j} + \bar{T}_{1j} \tag{64}$$

where

$$\bar{T}_{2j} \equiv \sum_{i=1}^{N+3} a_{ji}(q,t)\ddot{q}_i, \qquad \bar{T}_{1j} \equiv \frac{\mathrm{d}}{\mathrm{d}t}\left(\frac{\partial T}{\partial \dot{q}_j}\right) - \bar{T}_{2j} \tag{65}$$

Thus, the $(N+3)\times(N+3)$ matrix A, of Eqs. (62) and (63) has as its elements the a_{ji} of Eq. (65). A problem arises in extracting these elements for an arbitrary number of rods because $\ddot{\alpha}_n$ is often nested within a double summation with dependent indices. This difficulty is rectified by switching the order of summation according to the relationship

$$\sum_{i=1}^{N} m_i \sum_{n=1}^{i-1} b_n \ddot{\alpha}_n = \sum_{i=1}^{N}\left(b_i \sum_{n=i+1}^{N} m_n\right)\ddot{\alpha}_i \tag{66}$$

In this manner, the $\bar{T}_2$ terms can be written explicitly for N rods, as shown in Eq. (65). Again, for a detailed derivation, see Ref. 12.

The $\{B\}$ vector of Eq. (63) can be found by manipulation of Lagrange's equations:

$$B = \frac{\partial T}{\partial q_j} - \frac{\partial V}{\partial q_j} + Q_j - \bar{T}_{1j} \tag{67}$$

Here, A^{-1} can be determined either analytically or numerically to produce the final form of the equations of motion, as seen in Eq. (63).

Tether Forces

The tether forces at the attachment points to the orbiter and the probe can be easily computed using Newton's second law and solving

$$\boldsymbol{T} = m\boldsymbol{a} - \boldsymbol{F}_g - \boldsymbol{F} \tag{68}$$

where $\boldsymbol{T}$ is the tether force and $\boldsymbol{F}$ is the aerodynamic force acting on the particle, which for the orbiter and the probe are given in Eqs. (32) and (33), respectively. Here, $\boldsymbol{F}_g$ is the gravitational force, which can be obtained by

$$\boldsymbol{F}_g = -\mu m(\boldsymbol{R}/R^3) \tag{69}$$

Finally $\boldsymbol{a}$ represents the inertial accelerations of the probe and the orbiter, which are given by

$$\boldsymbol{a}_p = \left(\ddot{R}_p - R_p\dot{\theta}^2\right)\hat{c}_1 + (2\dot{R}_p\dot{\theta} + R_p\ddot{\theta})\hat{c}_2 \tag{70}$$

$$\begin{aligned}\boldsymbol{a}_o = {} & \left\{\ddot{R}_p - R_p\dot{\theta}^2 - \sum_{n=1}^{N} l_n\left[C\alpha_n(\dot{\alpha}_n+\dot{\theta})^2 + (\ddot{\alpha}_n+\ddot{\theta})S\alpha_n\right]\right. \\ & + \ddot{x}_s C\alpha_N - 2\dot{x}_s S\alpha_N(\dot{\alpha}_N+\dot{\theta}) \\ & \left. - x_s\left[C\alpha_N(\dot{\alpha}_N+\dot{\theta})^2 + (\ddot{\alpha}_N+\ddot{\theta})S\alpha_N\right]\right\}\hat{c}_1 \\ & + \left\{2\dot{R}_p\dot{\theta} + R_p\ddot{\theta} + \sum_{n=1}^{N} l_n\left[-S\alpha_n(\dot{\alpha}_n+\dot{\theta})^2 + (\ddot{\alpha}_n+\ddot{\theta})C\alpha_n\right]\right. \\ & + \ddot{x}_s S\alpha_N - 2\dot{x}_s C\alpha_N(\dot{\alpha}_N+\dot{\theta}) \\ & \left. - x_s\left[-S\alpha_N(\dot{\alpha}_N+\dot{\theta})^2 + (\ddot{\alpha}_N+\ddot{\theta})C\alpha_N\right]\right\}\hat{c}_2\end{aligned} \tag{71}$$

Numerical Results

In this section the tether aerocapture maneuver at Mars developed in Ref. 10 is simulated using a system of five hinged rods. The elastic properties of the tether (in particular, the stretching) are included in the analysis by setting the spring constant to[14]

$$k = E_t A_t / l \tag{72}$$

where A_t and E_t are the cross-sectional area and tensile modulus of the tether, respectively. (This spring constant is responsible for the so-called tether bounce phenomenon.) For the material in the Mars aerocapture tether (Hercules AS4), $E_t = 240$ GN/m^2, which results in an equivalent spring with $k = 71.2$ N/m. Damping effects are ignored at this stage. The initial conditions obtained from the rigid-rod analysis[10] are used in the multirod simulation, with the tether assumed to be initially straight and the spring in equilibrium. The results obtained from the single-rod simulation are presented again for comparison purposes (Figs. 3–5).

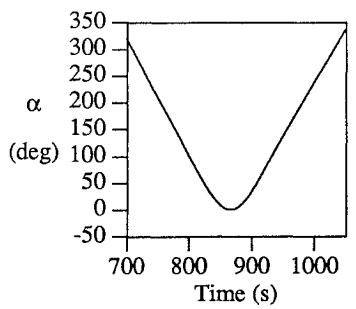

Fig. 3 Orientation angle (rigid rod).

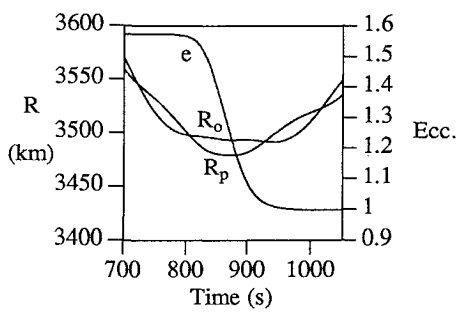

Fig. 4 Positions and eccentricity (rigid rod).

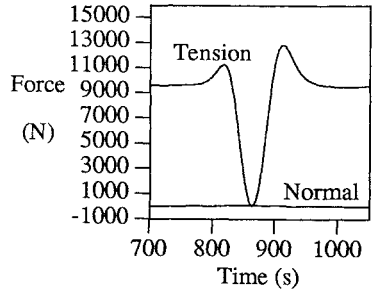

Fig. 5 Tether forces on probe (rigid rod).

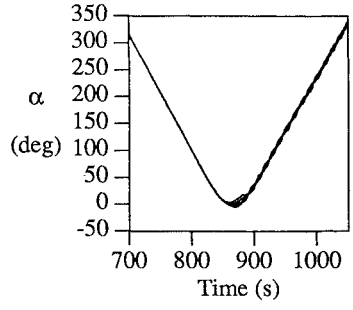

Fig. 6 Orientation angles (flexible).

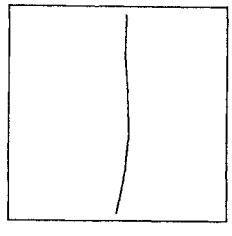

Fig. 7 Tether shape at 875 s.

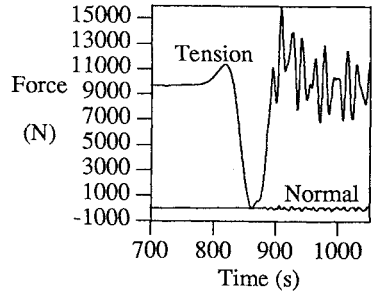

Fig. 8 Tether forces on probe (flexible).

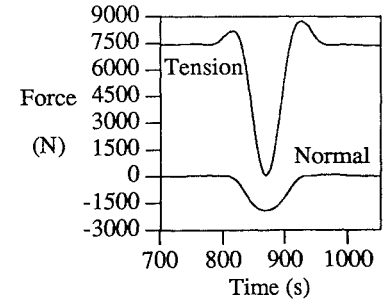

Fig. 9 Tether forces on probe (rigid rod).

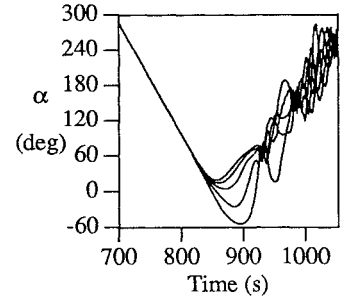

Fig. 10 Orientation angles.

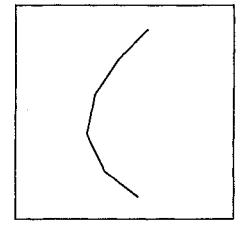

Fig. 11 Tether shape at 885 s.

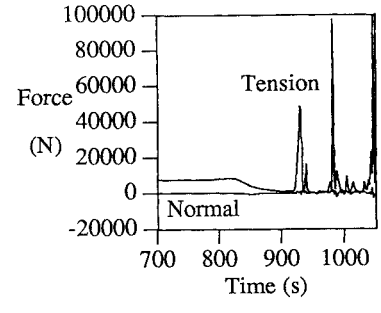

Fig. 12 Tether forces on probe (flexible).

Figures 3 and 6 show the orientation of the tethered system with respect to the local vertical. Before atmospheric impact, the five-rod system behaves as the single-rod model. During fly-through, between 825 and 925 s, bending occurs in the flexible model (see Fig. 6) and the plots for the five angles separate, indicating bending in the tether. The shape of the flexible tether at maximum bending (around 875 s) is shown in Fig. 7. Once bending has occurred in the flexible model, oscillations in the tether remain due to the lack of damping in the space environment. Note that if the bending effects are ignored, the spinning behavior of the two models is practically identical after impact.

The orbiter and probe distances from the center of the planet are plotted along with the eccentricity of the system in Fig. 4 for the rigid-rod model. Note that the radius of Mars is 3398 km, which is the minimum value shown in the plots. The corresponding behavior of the flexible system is nearly identical to that of Fig. 4. In both cases the orbiter remains approximately one tether length (12.4 km) higher than the probe during the maneuver. The eccentricities are also very similar for both cases.

Figures 5 and 8 show the tether forces on the probe. (The forces on the orbiter are very similar.) Behavior from initial conditions to capture conditions ($t \approx 925$ s) is virtually the same, so aerocapture is reliably modeled by the rigid rod. Note that in each plot there are two forces shown, namely the tension and normal force on the probe. The tension is largely due to spin rate and begins at approximately 10,000 N. At closest approach the tension drops to nearly zero (as does the spin rate) and then increases as the tether spins up during the exit phase. The normal force is nearly zero at all times due to the matching conditions (2) and (3) (otherwise, normal forces are possible with rigid-rod segments).

After aerocapture, we note that the hinged model presents larger tension forces. This is due to the appearance of bending during atmospheric impact. The large forces occur when the tether straightens due to spin-induced centrifugal forces. The oscillations in the tension forces coincide with the oscillations in the bending of the tether. Note that the oscillations also induce small normal forces in the tether. These could be reduced by increasing the number of rods in the simulation. The maximum value of the tension in the flexible tether is large enough to break the tether designed in Ref. 10 (see Table 1). However, the tension in the tether can be reduced with the introduction of damping in the model. Using a damping coefficient of 377 N-s/m, which approximates a critically damped system, the tension forces are reduced significantly and remain below 15,000 N during the maneuver (see Ref. 12). The oscillations of

the tether are damped out in this case, and the tension variations are reduced to a small value. The other characteristics of the maneuver are indistinguishable from those in the undamped case.

The results above indicate that the behavior of the flexible tether is very similar to that of the rigid rod when the matching conditions are met. This validates the rigid-rod model as a very useful tool in the preliminary design process. We conclude that the aerobraking tether remains feasible when flexibility is included in the analysis.

The flexible model provides a tool to determine the validity of the assumptions made[10] about the necessity to apply the matching conditions (2) and (3) in order to eliminate the normal forces. The center matching and aeromatching conditions can be easily unbalanced in the system above by changing the probe area to 100 m^2. Note that this dramatic change in area is picked to exaggerate the unbalancing. Naturally, in a real system, typical uncertainties (e.g., probe area uncertainty) will not result in significant unbalancing. The results of a Mars aerocapture maneuver into a near-parabolic orbit for this system are shown in Figs. 9–12. The rigid-rod results are similar to those in the previous section. The fly-through altitude is slightly lower and the tension forces are smaller, due to a lower spin rate (the smaller probe reduces the aerodynamic torque and thus the required spin rate to achieve a vertical fly-through orientation). Note that the spin matching condition was maintained as usual, to keep the tension force to a minimum.[10] However, one major difference exists: There are large normal forces on the rigid tether at periapsis (Fig. 9). At the same time, the tension forces are nearly zero due to the lack of spin. This indicates that large bending should occur in a flexible tether since the resultant force acting on the tether has a direction nearly perpendicular to it. The simulation of the same maneuver with a five-rod flexible model confirms this suspicion. The flexible system behaves like the rigid one until it reaches the atmosphere, where very large bending occurs, as can be seen in the angle plot (Fig. 10) and in the shape plot (Fig. 11). The bending radically changes the character of the maneuver in several ways. The effective length of the tether is reduced and the probe fly-through altitude is increased, which reduces drag forces. As a result the target eccentricity is never achieved and the system is not captured. In addition, extremely large forces appear in the tether (Fig. 12). As in the previous case the forces are caused by the tether straightening due to centrifugal forces, but the bending in this case is much more severe, resulting in an unacceptable maneuver.

This analysis validates the conjecture that the minimization of the normal forces in the rigid-rod model[10] is fundamental to the development of an acceptable (vertical dumbbell fly-through) maneuver. Additional numerical examples are provided in Ref. 12.

Conclusions

The equations of motion of an arbitrary number of linked rigid rods are very useful in analyzing the flexible behavior of a tether during aerocapture. Applications of these equations in numerical simulations allow critical questions to be answered about the magnitudes of the normal and tension forces in the tether and the shape of the tether during atmospheric fly-through. The results indicate that the tether aerocapture system remains feasible when a flexible tether is included in the analysis. The rigid-rod model is validated as an excellent tool for preliminary design.

Acknowledgment

Research of one of us (S. G. T.) was sponsored by Phillips Laboratory at Edwards Air Force Base through the U.S. Air Force Laboratory Fellowship Program.

References

[1]Penzo, P., and Ammann, P. (eds.), *Tethers in Space Handbook*, 2nd ed., Office of Space Flight Advanced Program Development, NASA, Washington, DC, 1989.

[2]Lorenzini, E., Grossi, M., and Cosmo, M., "Low Altitude Tethered Mars Probe," *Acta Astronautica*, Vol. 21, No. 1, 1990, pp. 1–12.

[3]Bergamaschi, S., and Bonon, F., "Equilibrium Configurations in a Tethered Atmospheric Mission," AAS/AIAA Astrodynamics Conf., Durango, CO, Paper AAS-91-543, Aug. 1991.

[4]Warnock, T., and Cochran, J., "Predicting the Orbital Lifetime of Tethered Satellite Systems," Forty-Third International Astronautical Federation Congress, Washington, DC, Paper IAF-92-0002, Aug.–Sept. 1992.

[5]Keshmiri, M., Misra, A., and Modi, V., "Effects of Aerodynamic Lift on the Stability of Tethered Subsatellite System," AAS/AIAA Spaceflight Mechanics Meeting, Pasadena, CA, Paper AAS-93-184, Feb. 1993.

[6]Krischke, M., Lorenzini, E., and Sabath, D., "A Hypersonic Parachute for Low-Temperature Reentry," Forty-Third International Astronautical Federation Congress, Washington, DC, Paper IAF-92-0822, Aug.–Sept. 1992.

[7]Puig-Suari, J., and Longuski, J. M., "Modeling and Analysis of Tethers in an Atmosphere," *Acta Astronautica*, Vol. 25, No. 11, 1991, pp. 679–686.

[8]Longuski, J. M., and Puig-Suari, J., "Hyperbolic Aerocapture and Elliptic Orbit Transfer with Tethers," Forty-Second International Astronautical Federation Congress, Montreal, Canada, Paper IAF-91-339, Oct. 1990.

[9]Puig-Suari, J., and Longuski, J. M., "Analysis of Aerocapture with Tethers," AAS/AIAA Astrodynamics Conference, Durango, CO, Paper AAS-91-549, Aug. 1991.

[10]Puig-Suari, J., Longuski, J. M., and Mechalas, J., "Aerobraking Tethers for the Exploration of the Solar System," Forty-Third International Astronautical Federation Congress, Washington, DC, Paper IAF-92-0001, Aug.–Sept. 1992 (also *Acta Astronautica*, Vol. 35, Nos. 2/3, 1995, pp. 205–214).

[11]Longuski, J. M., Puig-Suari, J., Tsiotras, P., and Tragesser, S., "Optimal Mass for Aerobraking Tethers," Forty-Fourth International Astronautical Federation Congress, Graz, Austria, Paper IAF-93-A.2.13, Oct. 1993 (also *Acta Astronautica*, Vol. 35, No. 8, 1995, pp. 489–500).

[12]Puig-Suari, J., "Aerobraking Tethers for the Exploration of the Solar System," Ph.D. Dissertation, School of Aeronautics and Astronautics, Purdue Univ., West Lafayette, IN, Aug. 1993.

[13]Greenwood, D. T., *Principles of Dynamics*, 2nd ed., Prentice–Hall, Englewood Cliffs, NJ, 1988.

[14]Longuski, J. M., "Preliminary Analysis of Structural Vibrations of a Tethered Satellite," Jet Propulsion Lab. Engineering Memorandum, EM 312/92-168, 1992.